EXPERIMENTAL CFD GRADE DATA FOR STRATIFIED TWO-PHASE FLOWS

C. Vallée, D. Lucas, M. Beyer, H. Pietruske, P. Schütz, H. Carl

Forschungszentrum Dresden-Rossendorf e.V., Institute of Safety Research,
D-01314 Dresden, Germany
Phone: +49 (0) 351 260 3227, Fax: +49 (0) 351 260 2818
c.vallee@fzd.de

Abstract

Stratified two-phase flows were investigated at two test facilities with horizontal test-sections. For both, rectangular channel cross-sections were chosen to provide optimal observation possibilities for the application of optical measurement techniques. In order to show the local flow structure, high-speed video observation was applied, which delivers the high resolution in space and time needed for CFD code validation.

The **H**orizontal **A**ir/**Wa**ter **C**hannel (HAWAC) is made of acrylic glass and allows the investigation of air/water co-current flows at atmospheric pressure and room temperature. At the channel inlet, a special device was designed for well-defined and adjustable inlet boundary conditions. For the quantitative analysis of the optical measurements performed at the HAWAC, an algorithm was developed to recognise the stratified interface in the camera frames. This allows to make statistical treatments for comparison with CFD calculation results. As an example, the instable wave growth leading to slug flow is shown from the test-section inlet. Moreover, the hydraulic jump as the quasi-stationary discontinuous transition between super- and subcritical flow was investigated in this closed channel. The structure of the hydraulic jump over time is revealed by the calculation of the probability density of the water level. A series of experiments show that the hydraulic jump profile and its position from the inlet vary sensibly with the inlet boundary conditions due to the momentum exchange between the phases.

The second channel is built in the pressure vessel of the TOPFLOW facility, which is used to perform air/water and steam/water experiments at pressures of up to 5.0 MPa and temperatures of up to 264°C, but under pressure equilibrium with the vessel inside. In the present experiment, the test-section represents a flat model of the hot leg of the German *Konvoi* pressurised water reactor scaled at 1:3. The investigations focus on the flow regimes observed in the region of the elbow and of the steam generator inlet chamber, which are equipped with glass side walls. An overview of the experimental methodology and of the acquired data is given. These cover experiments without water circulation, which can be seen as test cases for CFD development, as well as counter-current flow limitation experiments, representing transient validation cases of a typical nuclear reactor safety issue.

1. INTRODUCTION

In the event of a loss-of-coolant-accident (LOCA) in a pressurised water reactor (PWR), emergency strategies have to be mapped out, in order to guarantee a safe removal of the decay heat from the reactor core, also in case of component breakdown. In different scenarios of small break LOCA, stratified two-phase flow regimes can occur in the main cooling lines of pressurised water reactors. For instance, a natural co-current two-phase flow circulation can appear in the primary circuit or a counter-current flow in the hot leg during the reflux condenser mode. The intermittent flow regimes especially are relevant for the reactor safety. During the reflux condenser mode, high steam flow rates can for example induce slug flow and initiate a counter-current flow limitation (CCFL), which would affect the core cooling.

For the validation and optimisation of accident management strategies, such transient scenarios are reproduced in dedicated facilities or rather simulated. The use of one-dimensional system codes is state of the art, but these programs are not able to predict important flow conditions with the required accuracy and spatial resolution. In particular the CCFL conditions are dominated by 3D effects, which requires the use of a computational fluid dynamics (CFD) approach. However, the actual CFD codes applied to two-phase flows do not meet the high level of confidence needed in the field of nuclear reactor safety. Especially the closure models for turbulence and interfacial transfer embedded in CFD must be validated to allow reliable simulations. Therefore, high-resolution experimental data is needed for comparison with CFD calculations.

In order to support these tasks, two experimental facilities were built at Forschungszentrum Dresden-Rossendorf (*FZD*) for the investigation of stratified flows. The **H**orizontal **A**ir/**Wa**ter **C**hannel (HAWAC) is dedicated to generic co-current flow experiments at atmospheric pressure and room temperature. A special inlet device offers well-defined inlet boundary conditions for comparisons with CFD. Furthermore, a model of the hot leg of a PWR was installed in the pressure vessel of the TOPFLOW facility (Transient twO Phase FLOW) of *FZD*. The “hot leg model” allows the investigation of co- and counter-current flows under reactor typical boundary conditions (steam/water at pressures up to 5.0 MPa and saturation temperature). In both facilities, optical observation of the flow were performed and an algorithm was developed for the detection of the interface in the camera frames. Furthermore, statistical treatments of the data are presented showing the global structure of the interface, which can be used for comparison with CFD. This contribution gives an overview of the achieved results.

2. AIR/WATER EXPERIMENTS IN THE HAWAC TEST FACILITY

2.1. The Horizontal Air/Water Channel (HAWAC)

Experiments were carried out at the **H**orizontal **A**ir/**Wa**ter **C**hannel (Fig. 1), witch is devoted to co-current flows. A special inlet device provides defined inlet boundary conditions by a separate injection of water and air into the test-section. The test-section is 8 m long and its cross-section dimensions are 100 x 30 mm² (height x width). Therefore, the length-to-height ratio L/H is 80. Alternatively, related to the hydraulic diameter, the dimensionless length of the channel is $L/D_h = 173$.

The inlet device (Fig. 2) is designed for a separate injection of water and air into the channel. The air flows through the upper part and the water through the lower part of this device. Because the inlet geometry produces perturbations in the flow (bends, transition from pipes to rectangular cross-section), 4 wire mesh filters are mounted in each part of the inlet device. The filters are made of stainless steel wires with a diameter of 0.63 mm and have a mesh size of 1.06 mm. They aim at providing homogenous velocity profiles at the test-section inlet. Moreover, the filters produce a pressure drop that attenuate the effect of the pressure surge created by slug flow on the fluid supply systems.

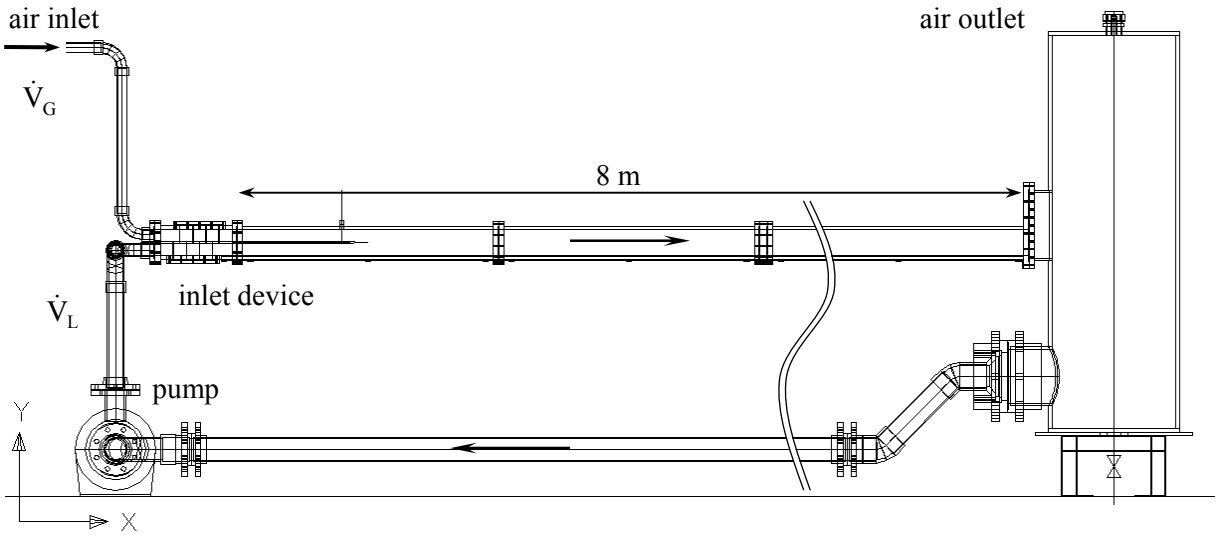

Fig. 1: Schematic view of the horizontal air/water channel (HAWAC)

Air and water come in contact at the final edge of a 500 mm long blade that divides both phases downstream of the filter segment. The free inlet cross-section for each phase can be controlled by inclining this blade up and down. The inclination of the blade is measured over the cross-section opening for the water (see red graduation in Fig. 2). Both, filters and inclinable blade, provide well-defined inlet boundary conditions for the CFD model and therefore offer very good validation possibilities.

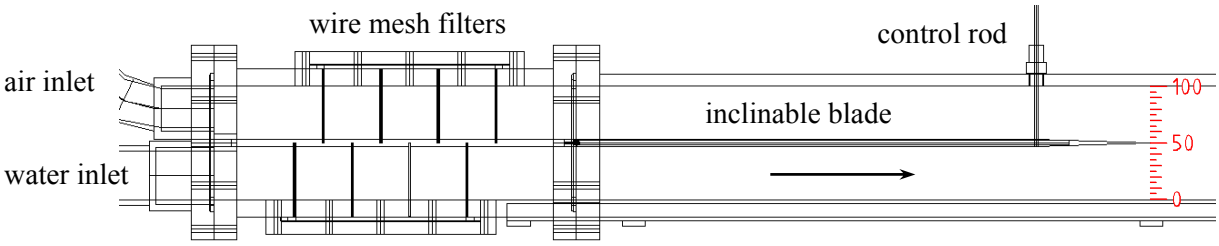

Fig. 2: The inlet device

The water flow rate is measured with a paddle-wheel flow transmitter and is adjusted via the frequency inverter of the pump motor. The air flow rate is measured and controlled with the thermal mass flow meters of the TOPFLOW-facility. These are mounted in parallel in order to ensure a high precision over a large measuring range. The flow rates are measured with an accuracy of ±0,2 l/s for the water and ±1,5% for the air. The maximum superficial velocities achieved in the test-section are 2 m/s for the water and 8 m/s for the air.

2.2. Flow regimes and flow pattern map of the HAWAC

A flow pattern map (Fig. 4) was arranged on the basis of visual observations of the flow structure at different combinations of the gas and liquid superficial velocities. The observed flow patterns are:

- 1 - stratified flow
- 2 - wavy flow
- 3 - elongated bubble flow
- 4 - slug flow

Further, sub-categories were defined to consider the slug generation frequency and the appearance of elongated bubbles in the channel:

- a - sporadic (transition regime)
- b - periodic, but only one type of structure (either slug or elongated bubble)
- c - periodic and several types of structure simultaneously

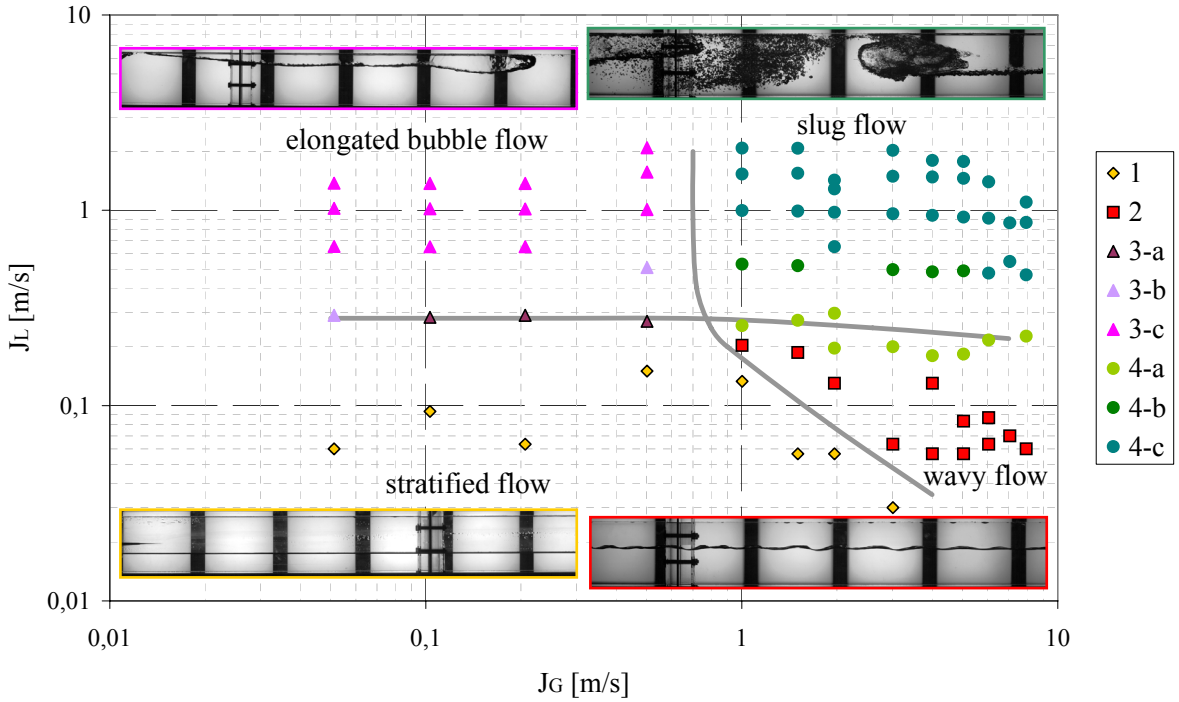

Fig. 4: Flow pattern map for the rectangular channel (inlet blade in horizontal position)

The adjustable inclination of the inlet blade separating the phases allows to influence the generation of the two-phase flow regime. The first contact between gas and liquid can be modified with the blade position: if the velocities at the end of the blade are similar, a smooth come together will be managed, else a perturbation can be introduced in the channel. Nevertheless, and despite a short channel length, the flow regime established at the end of the channel is not significantly affected by the blade inclination.

Furthermore, it was observed that the position of the inlet blade not always defines the water level at the channel inlet. For example when the inlet blade is inclined upwards and the water flow rate is very low, the water flow separates from the lower surface of the blade. In this case, the initial water level is lower than the height of the outlet edge of the blade. To create proper inlet boundary conditions at these flow rates, the blade has to be inclined down.

2.3. Optical measurements during slug flow

The presented experiment was focused on the generation of slug flow. It was performed at following superficial velocities in the test-section: j_L = 1.0 m/s for the water flow (i.e. 3.0 L/s) and j_G = 5.0 m/s for the air flow (i.e. 15.0 L/s). Further, the inlet blade was horizontal and therefore the cross-section opening at vertex of the inlet blade was 50 mm for each phase. Optical measurements were performed at the channel inlet with a high-speed video camera. The data presented in the following paragraphs is an example of the possibilities offered at the HAWAC facility.

2.3.1. High-speed video observations and interface capture

Due to the rectangular cross-section, the flow can be observed very well from the side of the duct. To make quantitative observations, the flow was filmed with a high-speed video camera at 400 frames per second. The following picture sequence (Fig. 5) shows an example of camera frames during slug generation.

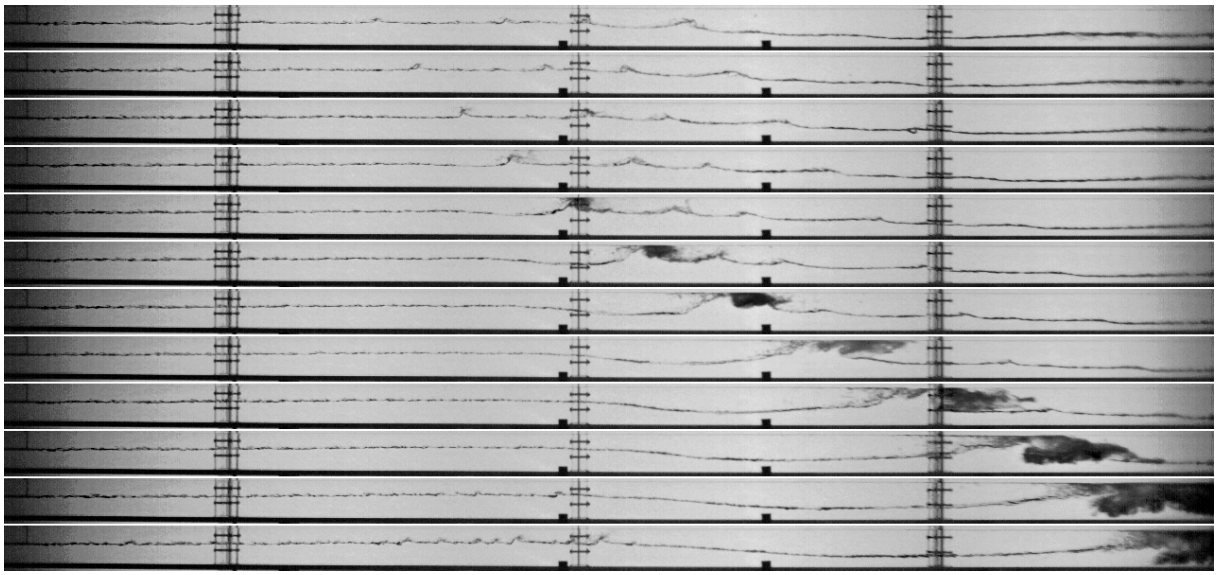

Fig. 5: Measured picture sequence at j_L = 1.0 m/s and j_G = 5.0 m/s with Δt = 50 ms
(depicted part of the channel: 0 to 3.2 m after the inlet)

To capture the gas-liquid interface in the camera frames, an image processing algorithm was developed. The capture method – illustrated in Figure 6 – consists in the following steps:

1. the synthesis of a background form the picture sequence by filtering out its dynamic component (Fig. 6-b);
2. a background subtraction with the image generated in step 1 (Fig. 6-c);
3. a pixel detection in each vertical line: - of the darkest pixel;
   - of the minimum of a grey-level time variation;
4. picking out of the pixels detected in step 3, the one which fits best into a continuous interface line (Fig. 6-d).

The capture method allows to represent the interface by a water level as function of the duct length z and the time t: $h(x, t)$. This data was tabulated in text files. The accuracy of the interface detection algorithm depends on the thickness of the interface in the images. In the stratified flow regions, the interface thickness is quite thin with at most 3 pixels. Therefore, the accuracy of the water level measurement is there about ±1.5 pixels. This corresponds to ±3.9 mm for a picture resolution of about 2.6 mm/pixel in this experiment.

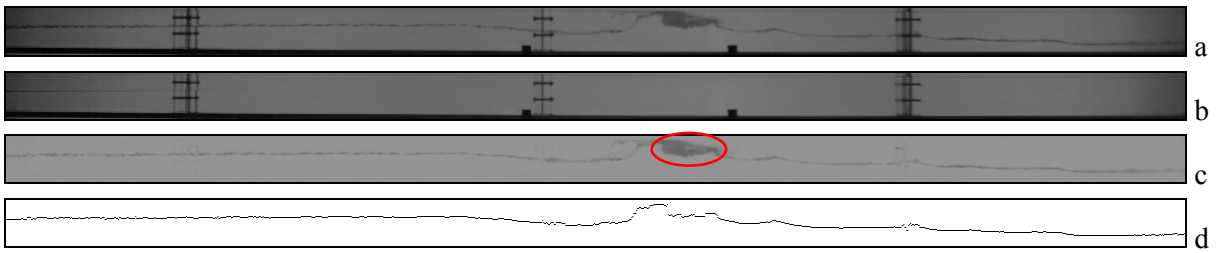

Fig. 6: Original picture (a), background picture (b), picture with subtracted background (c)
and detected interface during slug flow (d)

The accuracy is worse in the region of the slug front, where a two-phase mixture is generated (red circle in Fig. 6-c). This makes a definition of the water level difficult and induces sometimes unphysical fluctuations in the detected interface. In particular at the end of the visualised region (farther than 2.5 m from the inlet), where the slugs are developed, the interpretation of the water level measurement is delicate.

2.3.2. Water level measurement

The water level in a cross-section as a function of time can be extracted from the function *h(x, t)* by keeping *x* constant. The water level was measured with a frequency of 400 Hz, which corresponds to the frame rate of the high-speed camera. Figure 7 shows an example of the resulting water level history for six chosen cross-sections identified by a colour on the picture above. The indicated axial positions are taken from the final edge of the inlet blade. Close to the inlet, Figure 7 shows a rather constant water level which develops into a clear wavy flow at a distance of around 1.0 m. Downstream of 1.5 m, slugs are irregularly generated. With higher inlet length, the number of water level peaks decreases pointing out that some slugs merge together and some others collapse.

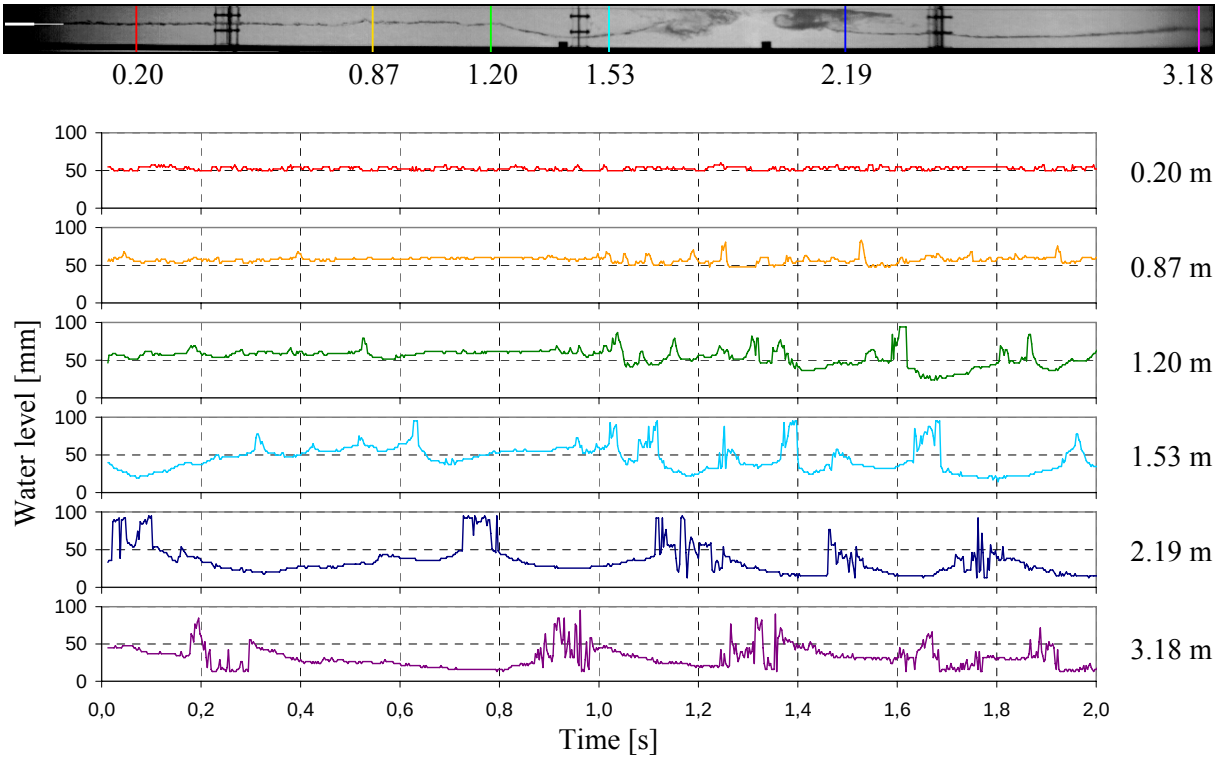

Fig. 7: Time-dependent water level in chosen cross-sections during slug flow (measuring frequency: 400 Hz)

2.3.3. Statistical treatment of the measured water levels for comparison with CFD

Since a direct comparison of the measured water levels with CFD results is difficult (how to synchronise both?), a statistical approach is proposed. First, a time averaged water level was calculated and bounded by the standard deviation in each cross-section (Fig. 8). This results in a mean water level profile along the channel which reflects the structure of the interface. Furthermore, the standard deviation σ quantifies the spread of the measured values which originates in the dynamic of the free surface.

In the first part of Figure 8, a slight increase of the mean water level from 50 mm at the inlet to 58 mm is observed as well as a low standard deviation. Both are characteristic for the supercritical flow ($Fr \geq 1$) obtained at the test-section inlet. In fact, in a supercritical flow the pressure drop due to wall friction results in an increase of the water level. Furthermore, only small supercritical waves can propagate in such a flow. Around the maximum of the mean water level reached at about 0.9 m from the inlet, the standard deviation increases quickly up to about 18 mm. This points out the rapid wave growth induced by the high air velocity in this zone. In the downstream region, where the slugs are generated and propagate, the mean water level decreases to an asymptotic value of about 30 mm. This shows an acceleration of the water flow, which can be attributed to the momentum exchange between the phases.

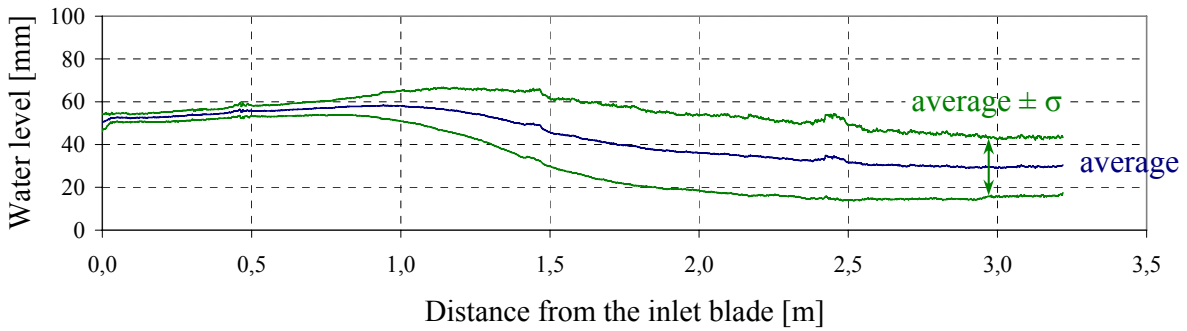

Fig. 8: Time averaged water level bounded by the standard deviation

2.4. Investigations on the hydraulic jump in a closed channel

2.4.1. The hydraulic jump phenomenon

The hydraulic jump is the discontinuous transition between super- and subcritical flow, and is well-known in open channel flow (e.g. Henderson, 1966). As shown in Figure 9, it is characterised by a steep rising of the water surface with a high turbulence zone and possible gas entrainment.

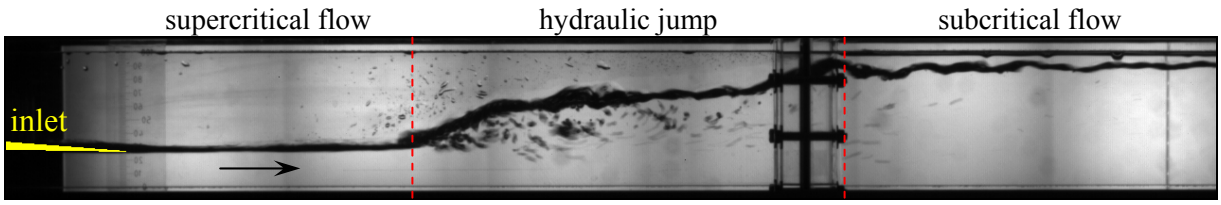

Fig. 9: Side view of a hydraulic jump in a horizontal channel

The classical approach for open channel flows (Hager, 1992) defines the flow conditions in a cross-section with the Froude number:

$$Fr = v / c \tag{1}$$

where v is the averaged cross-sectional velocity and c the celerity of shallow water waves, which are commonly expressed as follows:

$$v = \frac{\dot{V}}{W \cdot h} \tag{2}$$

$$c = \sqrt{g \cdot h} \tag{3}$$

Here, $\dot{V}$ is the water volume flow rate, W the channel width, h the water level and g the gravitational acceleration.

The subcritical flow is defined by $Fr < 1$, which means that waves can propagate downstream as well as upstream. The supercritical flow is characterised by $Fr > 1$ and implies that waves can only propagate downstream. Therefore, a perturbation cannot influence the flow in the upstream direction: a supercritical flow is upstream controlled. In the hydraulic jump, the kinetic energy of the supercritical flow is converted into potential energy, leading to the steep rising of the water level, and into heat over the turbulent energy dissipation.

Contrary to the hydraulic jump in open channel flows, in conduits the jump height is limited. Moreover, an air flow in the conduit possibly influences the jump over interfacial momentum transfer. Therefore, combined with the high turbulence dissipation, the hydraulic jump is an interesting quasi-stationary test case for two-phase flow models.

2.4.2. Experimental methodology

Optical measurements were performed with a high-speed video camera at 60 frames per second and the interface capture method presented in section 2.3.1. was applied to the pictures of the hydraulic jump. A resolution of about 0.75 mm/pixel was obtained in these experiments. As mentioned previously, the accuracy of the interface detection algorithm depends on the thickness of the interface in the images. In the stratified flow regions, the interface thickness is quite thin with at most 10 pixels. Therefore, the accuracy of the water level measurement is there about ±5 pixels, which corresponds to ±3.7 mm. The accuracy is worse in the turbulent region of the hydraulic jump, in particular when bubbles are entrained in the liquid phase. In such cases, the interface may be more than 20 pixels thick, which sometimes induces higher fluctuations in the detected interface.

The hydraulic jump realised in the HAWAC test-section is a stationary phenomenon. However, the interface is very dynamic because of the high turbulence in the jump. Therefore, a statistical approach is proposed in order to reflect the structure of the interface over time. The probability distribution of the water levels was calculated in each vertical cross-section for the complete measuring time. The number *n(x, y)* of water levels measured at the pixel with the coordinates *(x, y)* were summed up over the total number of frames *N* and the probability density *p* was calculated as follows:

$$p(x,y) = \frac{n(x,y)}{N} \tag{4}$$

Since for each frame, one single water level is detected in each vertical line, the sum of the probabilities in a cross-section *x* is equal to unity:

$$\forall x = \text{const}, \sum_{y=0}^{y=H} p(x,y) = 1 \tag{5}$$

As an example, one of the experiments was chosen to represent the calculated probability distributions according to a coloured scale (Fig. 10). This run was performed at following boundary conditions:

- water flow rate: 1.4 L/s (i.e. j_L = 0.47 m/s)
- air flow rate: 1.55 L/s (i.e. j_G = 0.516 m/s)
- inlet blade position: 26/74 mm (water/air)

Figure 10 shows thin distributions with high probability densities in the supercritical flow region, indicating a relatively stable interface. The beginning of the hydraulic jump is smeared and the probability decreases accordingly, which reveals the high turbulence in the interfacial area. In the second part of the flow transition, the distributions become thinner and the probability higher.

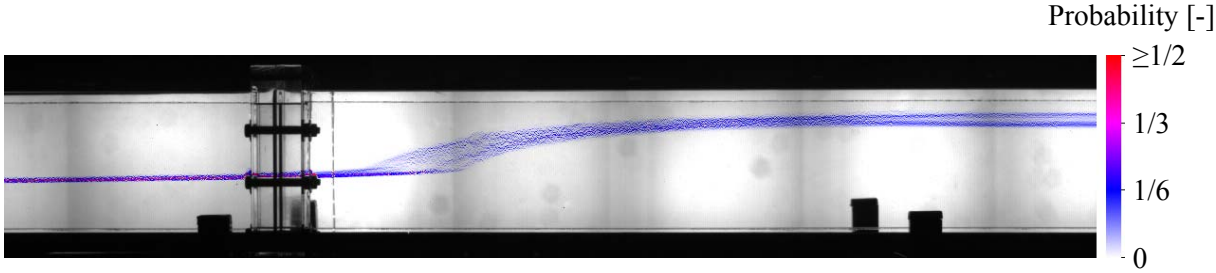

Fig. 10: Representation of the probability density of the water level measured in a hydraulic jump (colours) over a picture of the background (black and white) for *N* = 672 frames (i.e. 11.2 s)

2.4.3. Influence of the air flow rate on the hydraulic jump

Experimental series were focused on the influence of the air flow rate on the hydraulic jump. Therefore, these experiments were performed at constant inlet boundary conditions for the water: the water flow rate was 1.4 L/s (i.e. superficial velocity in the test-section j_L = 0.47 m/s) and the inlet blade was inclined down to an inlet height of 26 mm for the water. At these conditions, a Froude number of about 3.6 is achieved in the inlet cross-section, which indicates a clear supercritical flow. Moreover, the cross-section opening for the air was 74 mm. Optical measurements were performed by variation of the air flow rate and were analysed using the methodology presented in the previous section.

The probability distributions of the water level were calculated for each run and are presented in Figure 11. Because the camera had to be moved during the experiments, the pictures show different parts of the test-section. For a simple comparison between the runs, the pictures were arranged in Figure 11 according to their relative position (reference flange at x = 1.5 m). At first, Figure 11 shows the strong dependence of the hydraulic jump axial position on the air flow rate. The hydraulic jump distance from the inlet was read out of the single pictures representing the probability distribution. Because this distance varies during the measuring time, the minimum and maximum axial positions were plotted in function of the air superficial velocity in Figure 12. This shows the increase of the hydraulic jump distance from the inlet with the air flow rate, pointing out the influence of the momentum exchange between the phases on the jump position. Furthermore, the increasing distance between minimum and maximum positions reflects the increasing smearing of the area where the jump begins with higher air flow rate. As shown in (Vallée, 2007-b), these increasing fluctuations point out the influence of the flow regime downstream of the hydraulic jump: during slug flow, larger amplitudes were observed than during elongated bubble flow.

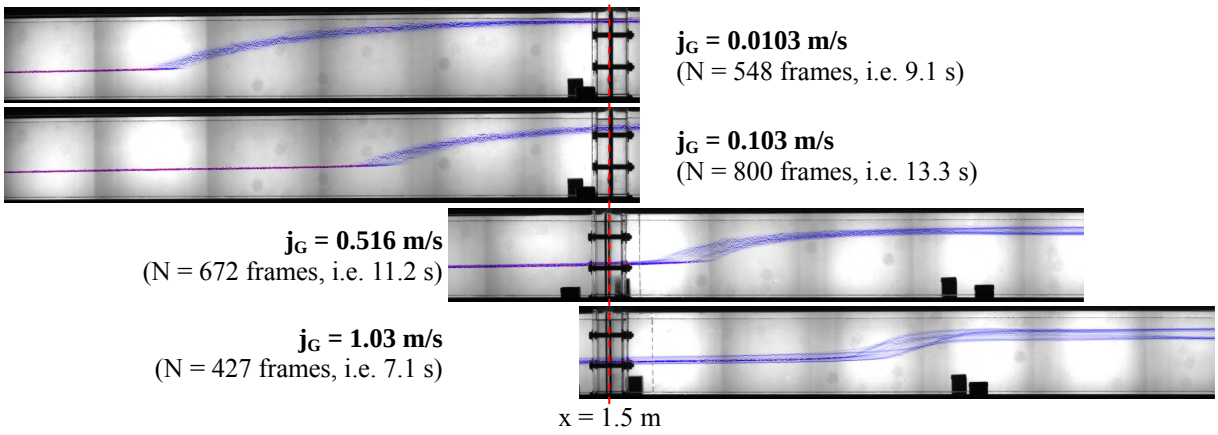

Fig. 11: Influence of the air flow rate on the hydraulic jump represented by the probability density

Moreover, Figure 11 shows an increase of the water level immediately before the hydraulic jump with higher air flow rate. This is due to the frictional pressure drop, which increases the water level in flow direction when Fr > 1. The variation of the water level immediately before the jump induces a variation of the Froude number, which is characteristic for the jump. As a result of the increasing water level, the Froude number at the jump beginning decreases with higher air flow rate. The decreasing Froude number results in a change of the jump appearance: the jump becomes flatter and its beginning smoother. This is qualitatively in agreement with studies conducted in open channel flows (Henderson, 1966) and with the experiments made by Stahl and Hager (1999) in a pipe.

A test matrix consisting of 75 runs is available with variation of the inlet blade position between 15 and 55 mm for the water, with water flow rates ranging from 1.0 to 3.0 L/s (i.e. j_L = 0.34 to 1.0 m/s) and air flow rates from 0.03 to 7.5 L/s (i.e. j_G = 0.010 to 2.5 m/s).

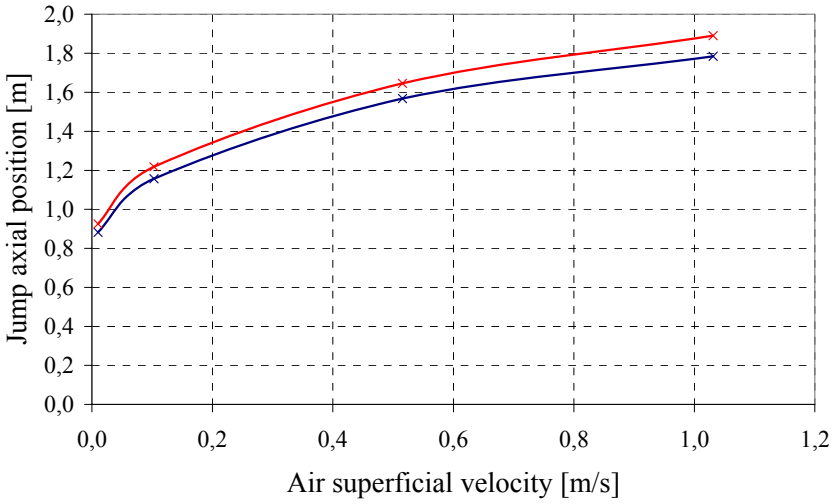

Fig. 12: Variation of the jump position (min/max)

3. EXPERIMENTS IN THE HOT LEG MODEL OF THE TOPFLOW FACILITY

3.1. The hot leg model

The test section of the hot leg model is schematically shown in Figure 13. The main components consist of the test section itself, the reactor pressure vessel (RPV) simulator located at the lower end of the horizontal channel and the steam generator (SG) separator connected to the SG inlet chamber. The test section reproduces the hot leg of a pressurised water reactor from the German *Konvoi* type at a scale of 1:3. In order to provide optimal observation possibilities, the test section is not composed of pipes like in the original power plant, it is a 50 mm thick channel representing a cut through the vertical mid-plane of the hot leg and of the steam generator inlet chamber. Consequently, the test section is composed of a horizontal rectangular channel, a bend that connects it to an upward inclined and expended channel, and a quarter of a circle representing the steam generator inlet chamber. The horizontal part of test section is 2.12 m long and has a rectangular cross section of 0.05 x 0.25 m². The SG and RPV simulators are identical vessels with 0.8 x 0.5 x 1.55 m³ (D x W x H) cubic shape.

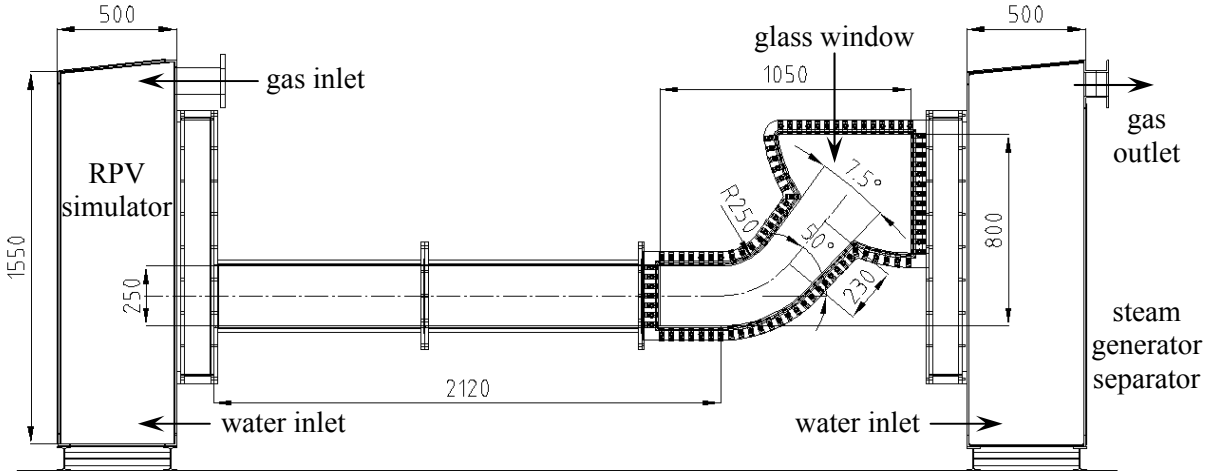

Fig. 13: Schematic view of the hot leg model test section (dimension in mm)

In order to visualise the flow over big size windows at high pressures, the hot leg model is operated under pressure equilibrium. This condition is realised in the pressure vessel of the TOPFLOW facility of *FZD* (Fig. 14), where the test section is installed in. For steam/water experiments, a special heat exchanger condenses the exhaust vapour from the test section directly in the pressure vessel. As shown in Figure 14, the cold end of this condenser is permanently connected with the inside atmosphere of the vessel in order to guarantee full pressure equilibrium at all times (Prasser, 2006). The vessel can be pressurised up to 5 MPa either with air for cold experiments or with nitrogen for steam experiments. Thanks to this method, the test section does not have to support overpressures and can be designed with thin materials. Furthermore, this allows to equip the test section with glass side walls for visual observations. This is realised in the bended region of the hot leg and of the steam generator inlet chamber as shown in Figure 13. The flow behaviour was recorded by a high-speed video camera at frequencies of 60 to 100 Hz and a shutter speed of 1/500 to 1/1000 s during 40 to 180 s.

Furthermore, global parameters were measured via a data acquisition system running at 1 Hz, which was synchronised with the camera. A vortex meter was used to measure the injected water mass flow rate. The injected air mass flow rate was measured and controlled using thermal mass flow meters, the steam flow rate over the pressure drop through a Venturi tube. The temperature of the fluids were measured by thermocouples at various positions in the facility. Furthermore, the water levels in both separators were determined by the measurement of the differential pressure between the top and the bottom of the vessels with differential pressure transducers. The pressure drop over the test section was measured by a differential pressure transducer placed between the SG and RPV separators. These global parameters give important input or output values for the comparison with simulations.

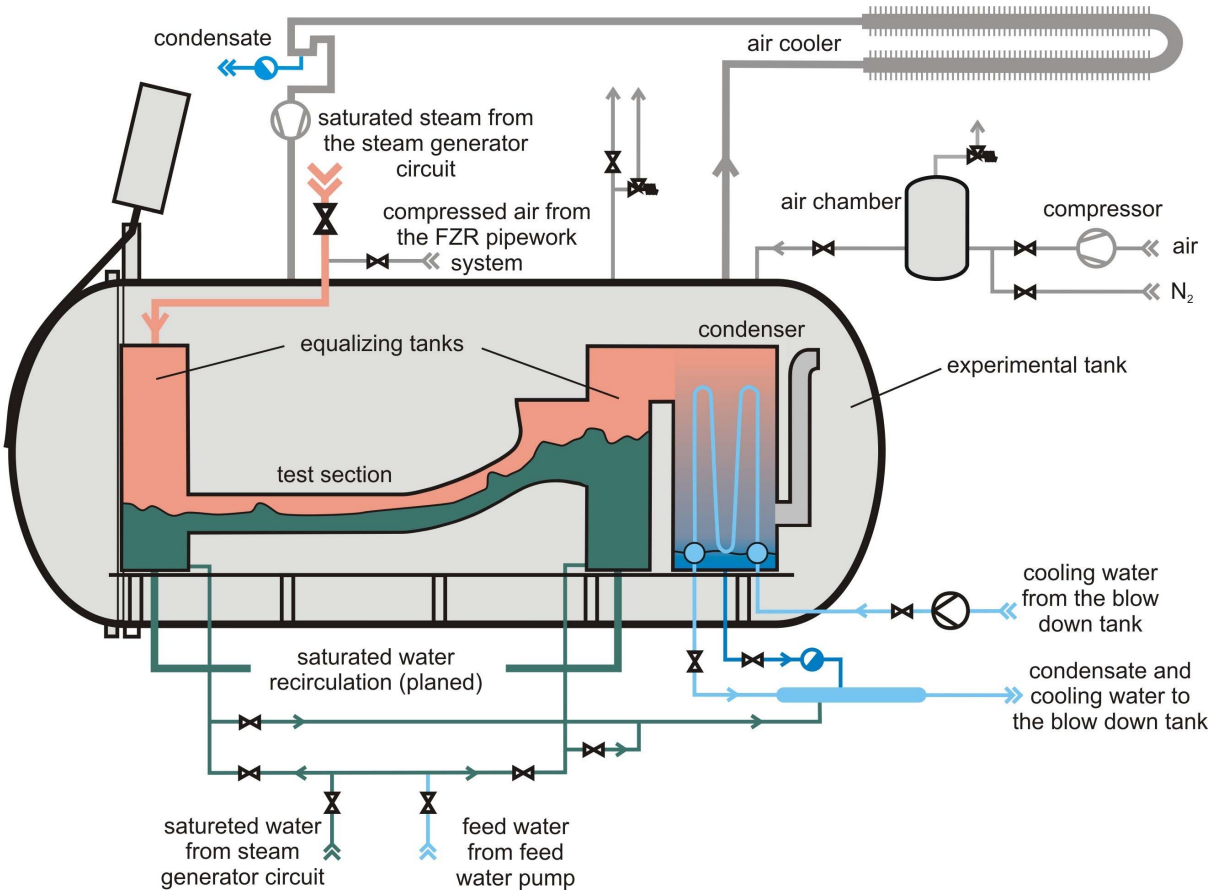

Fig. 14: Schematic view of the experimental apparatus

3.2. Hot leg experiments

The following types of experiments were performed with air/water as well as steam/water:

- Experiments without water circulation for CFD validation purposes: the test section is filled with a certain amount of water and a constant gas flow rate is injected. The gas flowing through the hot leg model entrains the stagnant water, analogical to bubble column experiments.
- Simulation of the co-current two-phase flow natural convection: different combinations of water and gas flow rates are injected in the RPV simulator and flow to the SG separator. The water flow rate to the SG separator can be evaluated from the water level increase in this vessel.
- Generic investigation of counter-current flows for CFD validation purposes: water is injected from the SG side and flows through the test section to the RPV simulator, which is filled. When the water level in the RPV simulator and in the horizontal part of the hot leg is high enough, waves and slugs are generated and inhibit the water to flow to the RPV simulator. Therefore, the injected water accumulates in the SG separator. Theses experiments were repeated with different combinations of water and gas flow rates.
- Simulation of the reflux condenser mode and counter-current flow limitation: a constant water flow rate is injected in the SG separator and flows to the test section whereas the gas flow rate is stepwise increased up to CCFL conditions. The limitation of the water flow rate streaming through the test section (discharge water flow) is evaluated over the increase of the water level in the RPV simulator. Therefore, the water level in this separator is kept below the inlet nozzle of the hot leg.
- Simulation of deflooding conditions during reflux condenser mode: a constant water flow rate is injected in the SG separator and a high gas flow rate is injected in order to establish CCFL conditions. During a run, the gas flow rate is stepwise decreased until the breakdown of the CCFL and the achievement of a stable counter-current flow. Like in the flooding experiments, the water level increase in the RPV separator indicates the discharge water flow rate.

For all types of quasi-stationary experiments (all apart from the CCFL experiments), the test matrix was build in order to be able to cross different parameters: points with equal mass flow rate, equal superficial velocity and equal Wallis parameter were chosen. This allows to check the possible similarities involving these parameters for the experiments performed at different pressures. The boundaries of the parameters relevant for the experiments are indicated in table 1.

Table 1: Main characteristics of the hot leg experiments

experiments	pressures	temperature	water flow rates [2]	gas flow rates [2]	total runs
air/water	3.0 bar [1]	room	0.3 - 0.9 kg/s	10 - 145 g/s [3] 180 - 340 g/s [4]	66
steam/water	1.5; 3.0; 5.0 MPa	saturation	0.3 - 0.9 kg/s	35 - 1200 g/s	125

Notes: 1. some single experiments were repeated at 1.5 and 5.0 bar
2. minimum and maximum values
3. for the quasi-stationary experiments
4. for the transient CCFL experiments

3.3. Example of counter-current flow experiment

As an example, a counter-current flow experiment was chosen to illustrate the available data. This run was performed at a system pressure of 3.0 MPa and a temperature of about 232°C, which is close to the saturation conditions. The mass flow rates were 0.85 kg/s for the water and 0.20 kg/s for the steam. Figure 15 shows the evolution of the water level in the separators and of the pressure drop over the test section. Before the beginning of slug flow generation in the test-section ($t \leq 20$ s), the water injected in the SG separator flows through the test section to the RPV simulator (Fig. 16-a). Therefore, the water level in the SG separator is constant at about 0.86 m and the water level in the RPV simulator increases. At about $t = 20$ s, the water level reached in the horizontal part of the hot leg obstructs the steam flow enough to generate waves at the interface, which finally grow to slugs (Fig. 16-b). Consequently, the pressure difference between the separators increases and becomes unstable. Afterwards, the gas hindering the water to flow to the RPV, it accumulates in the SG separator. The mean pressure drop over the test section increases with the water level in the SG and the slugs become bigger (Fig. 16-c).

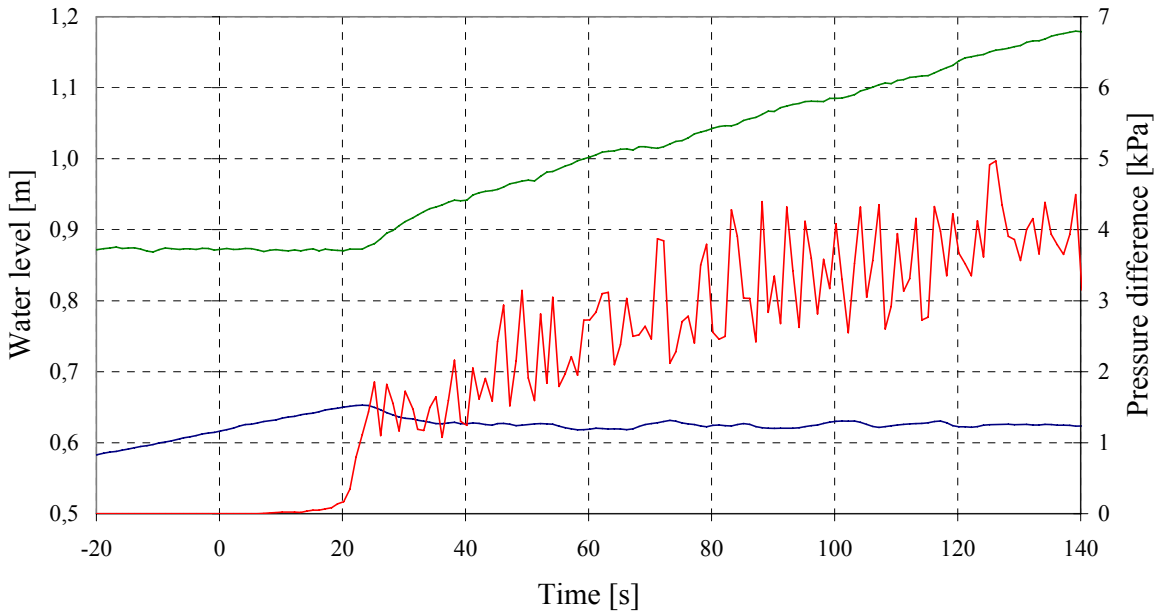

Fig. 15: Evolution of the water level in the RPV simulator (in blue) and SG separator (in green) and of the pressure difference (in red) during a counter-current flow experiment at 3.0 MPa with $\dot{m}_L = 0.85$ kg/s and $\dot{m}_G = 0.20$ kg/s

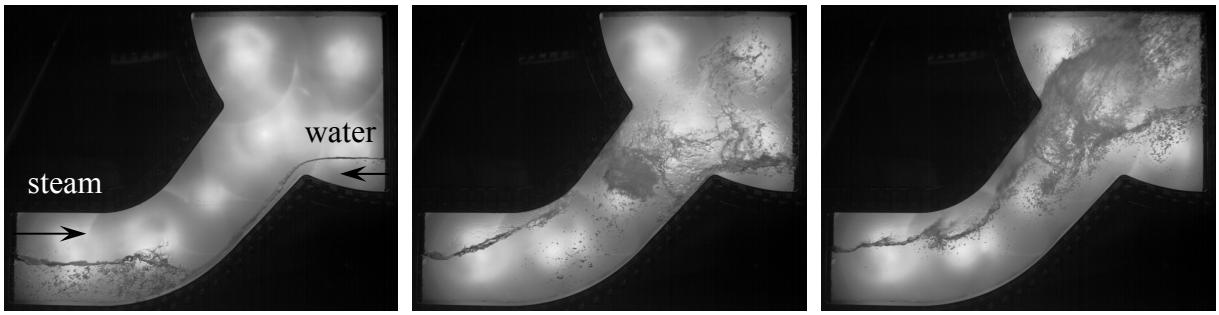

a) t = 0.00 s b) t = 23.00 s c) t = 80.00 s

Fig. 16: Evolution of the flow during the steam/water counter-current flow experiment performed at 3.0 MPa with $\dot{m}_L$ = 0.85 kg/s and $\dot{m}_G$ = 0.20 kg/s

3.4. Comparison with other counter-current flow experiments

As an example, a series of counter-current flow experiments performed at similar Wallis parameters J^* were compared. For the phase i, this dimensionless superficial velocity is given by:

$$J_i^* = j_i \cdot \sqrt{\frac{\rho_i}{g \cdot H \cdot (\rho_L - \rho_G)}} \tag{6}$$

where j is the superficial velocity and ρ the density of the fluid, g the gravitational acceleration and H the channel height.

The boundary conditions of the compared experiments are given in table 2. The flow rates correspond to a Wallis parameter of about 0.050 for the water and about 0.094 for the gas. Figure 17 shows high-speed camera pictures of the flow after an accumulation of water in the SG separator of about 1.0 m (i.e. at t = 60 s for the 3.0 MPa experiment – see Fig. 15). The aspect of the flow shown at different boundary conditions presents qualitative similarities. However, because of the unsteady character of slug flow, a detailed analysis of various global parameters is necessary to confirm these results. Furthermore, the application of image processing methods to the picture sequences like those presented in section 2 could deliver local information in order to complete this analysis.

Table 2: Boundary conditions of the compared counter-current flow experiments

gas / run number	air / 24-12	steam / 17-13	steam / 13-08	steam / 15-15
pressure [MPa]	0.3	1.5	3.0	5.0
temperature [°C]	20 - 25	197	232	262
gas flow rate [kg/s]	0.108	0.15	0.20	0.25
water flow rate [kg/s]	0.90	0.90	0.85	0.80

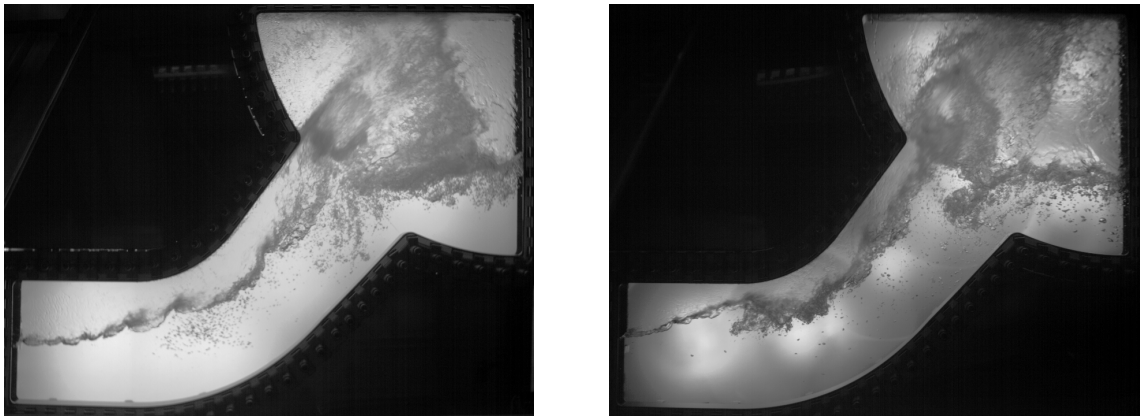

a) air/water – 0.3 MPa b) steam/water – 1.5 MPa

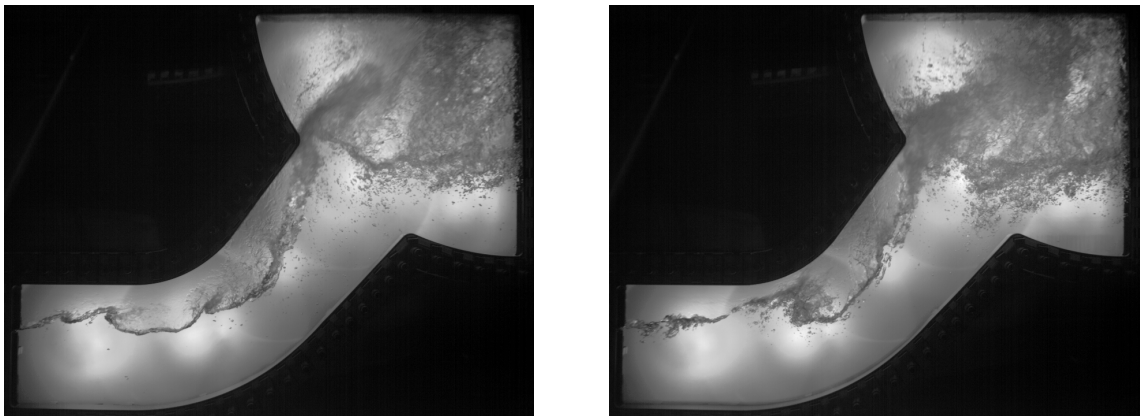

c) steam/water – 3.0 MPa d) steam/water – 5.0 MPa

Fig. 17: Example of images obtained at different pressures during counter-current flow experiments

4. COMPARISON WITH CFD SIMULATIONS

The high-speed camera pictures of the flow presented in the previous sections can be used directly for qualitative comparison with CFD. For more detailed analysis based on local information, quantitative results can be obtained from the application of the interface capture algorithm presented in section 2.3.1. However, a comparison of these data with simulation results requires the definition of a surface similar to the interface observed in the camera pictures. This is evident for interface tracking methods (e.g. volume of fluid method) but necessitates actually to make assumptions while using methods without sharp interface modelling like the two-fluid model. In this case, one possibility could be to model the smeared appearing interface with an isosurface of void fraction. Afterwards, statistical treatments can be applied to the coordinates of this surface over time, exactly like for the experimental data, in order to compare both. The treatments proposed in this paper are the calculation of the averaged flow profile during slug flow (Fig. 8) or the representation of the probability density of the water level measured in a hydraulic jump (Fig. 11).

Such a quantitative comparison was shown for the slug flow experiment in (Höhne & Vallée, 2008). Furthermore, this test case was calculated within the frame of the European NURESIM project with *FLUENT* at the *Université catholique de Louvain* (UCL), *NEPTUNE_CFD* at Électricité de France (EDF) and *ANSYS-CFX* by FZD. A comparison of the different simulation results with the experiment is given by Y. Bartosiewicz (2008). Moreover, pre-test calculations of hot leg model experiments were performed with *ANSYS-CFX* (Vallée et al., 2007-a). A comparison with the now available experimental results is planed.

Not least, the presented HAWAC slug flow experiment was selected as benchmark case for primary circuits by the OECD/NEA-CSNI working group on the analysis and management of accidents (GAMA).

5. SUMMARY AND CONCLUSIONS

For the investigation of co-current two-phase flows, the horizontal air/water channel (HAWAC) was built at *Forschungszentrum Dresden-Rossendorf* (FZD). A special inlet device provides well defined as well as variable boundary conditions and therefore very good CFD code validation possibilities. A flow pattern map was arranged to show the potential of the HAWAC facility. Optical measurements were performed with a high-speed video camera. By an interface capture method, the water level can be measured in each observed cross-section. Afterwards, the water level history can be extracted from the image sequences. Further, statistical treatments of the data are proposed for a comparison of the interface structure with CFD. The evolution of the time averaged water level bounded by the standard deviation was shown along the channel during slug generation. For investigations on the hydraulic jump in a closed channel, a representation of the probability density of the water levels was used.

Furthermore, the TOPFLOW facility of *FZD* was extended by a new test section representing a flat model of the hot leg of the German *Konvoi* pressurised water reactor scaled at 1:3. The "hot leg model" is installed in a pressure vessel and is operated in pressure equilibrium with the inside atmosphere. This technique allows optical observation of two-phase flows over big size windows at pressures up to 5.0 MPa. Therefore, local flow information can be acquired under reactor typical boundary conditions (saturated steam/water flow) for CFD validation purposes. Different types of experiments were performed with air or steam and water in co- and counter-current by variation of the pressure and flow rates. An overview of the experimental methodology and of the recorded data was given. On one hand, the experiments without water circulation are dedicated test cases for CFD development. On the other hand, the counter-current flow limitation experiments represent challenging transient validation cases of a typical nuclear reactor safety issue. Exemplary pictures of the flow observed in the region of the elbow and of the steam generator inlet chamber were presented.

In the next future, a detailed analysis of the global parameters (boundary conditions) acquired at the hot leg model is planed. Furthermore, the application of interface detection algorithms to the high-speed camera pictures would allow to access to quantitative local flow information.

NOMENCLATURE

Sign	Unit	Denomination
c	m/s	celerity of shallow water waves
Fr	-	Froude number
g	m/s²	gravitational acceleration
H	m	channel height
h	m	water level
J	-	Wallis parameter
j	m/s	superficial velocity
L	m	channel length
$\dot{m}$	kg/s	mass flow rate
N	-	number of frames
p	-	probability
t	s	time
$\dot{V}$	m³/s	volume flow rate
v	m/s	velocity
W	m	channel width
x	m	horizontal coordinate
y	m	vertical coordinate
ρ	kg/m³	fluid density
σ	-	standard deviation

Indexes:

G	gaseous phase
L	liquid phase

Abbreviations:

CCFL	counter-current flow limitation
HAWAC	**H**orizontal **A**ir/**Wa**ter **C**hannel of the *FZD*
LOCA	loss-of-coolant-accident
PWR	pressurised water reactor
RPV	reactor pressure vessel
SG	steam generator
TOPFLOW	**T**ransient **T**w**o** **P**hase **Flow** test facility of the *FZD*

REFERENCES

Y. Bartosiewicz, J.-M. Seynhaeve, C. Vallée, T. Höhne, J.-M. Lavieville, "Modelling free surface flows relevant to a PTS scenario: comparison between experimental data and three RANS based CFD-codes - Comments on the CFD-experiment integration and best practice guideline", XCFD4NRS - Experiments and CFD Code Applications to Nuclear Reactor Safety, 10.-12.09.2008, Grenoble, France (2008)

W. H. Hager, "Energy dissipators and hydraulic jump", Kluwer academic publishers, Dordrecht, Netherlands (1992)

T. Höhne & C. Vallée, "Numerical prediction of horizontal stratified flows", 6th International Conference on CFD in Oil & Gas, Metallurgical and Process Industries, 10-12 June 2008, Trondheim, Norway, Paper N° CFD08-12 (2008)

F. M. Henderson, "Open channel flow", The Macmillan compagny, New York (1966)

H.-M. Prasser, M. Beyer, H. Carl, A. Manera, H. Pietruske, P. Schütz, F.-P. Weiß, “The multipurpose thermalhydraulic test facility TOPFLOW: an overview on experimental capabilities, instrumentation and results”, Kerntechnik 71-4, 163-173 (2006)

H. Stahl & W. H. Hager, “Hydraulic jump in circular pipes”, Can. J. Civ. Eng. 26, 368-373 (1999)

C. Vallée, T. Höhne, H.-M. Prasser & T. Sühnel, “Experimental investigation and CFD simulation of slug flow in horizontal channels”, Forschungszentrum Dresden-Rossendorf, FZD-485 (2007-a)

C. Vallée, “Hydraulic jump in a closed horizontal two-phase flow channel”, International Conference on Multiphase Flow 2007, 09-13 July 2007, Leipzig, Germany, Paper N° S5_Fri_A_63 (2007-b)

ACKNOWLEDGEMENTS

This work is carried out in the frame of a current research project funded by the German Federal Ministry of Economics and Labour, project number 150 1329.

The authors would like to thank the TOPFLOW team for their work on the test facility and the preparation of the experiments, by name Klaus Lindner, Heiko Rußig, Marko Tamme and Steffen Weichelt.